GENERAL CIRCULATION: MEAN CHARACTERISTICS (MS 154)

Richard Grotjahn,

Richard Grotjahn
Department of Land, Air, and Water Resources,
One Shields Ave
University of California,
Davis, California 95616-8627, USA
grotjahn@ucdavis.edu
5307522246 (V)
5307521793 (F)

Abstract/Synopsis
The large scale average conditions of the atmosphere are described. Emphasis is placed on the primary observed variables: radiation, temperature, pressure, wind, clouds, and precipitation rate. Zonal and time average fields as well as time average fields at representative levels are shown.

1.1 INTRODUCTION

The atmosphere of the Earth has a diverse range of motions. The general circulation refers to the larger scale motions having horizontal length scales greater than 1000 km and persisting for a season or longer. In addition, this subject includes all processes necessary to explain sufficiently, or maintain directly, the large scale circulation.

The general circulation is a broader subject than simply the large scale movement of air. Understanding the circulation requires examination of other atmospheric quantities. The large scale circulations are created by imbalances in the radiation fields that lead to temperature gradients that the atmosphere tries to eliminate. The circulations that develop are limited by various physical constraints such as radiative energy balance, mass balance, and angular momentum balance. So, while the primary scope of this article is to display the average properties of the circulation, it is also necessary to consider related variables that are directly observed. The related variables are connected by constraints and the underlying laws of dynamics and thermodynamics. Other articles on the general circulation discuss how the circulation is maintained and how it can be simulated.

The general circulation of the atmosphere has complex structure in all dimensions as it evolves over the seasons. However, the Earth rotates fast enough relative to the radiative response time of much of the atmosphere so that many properties of the atmosphere have a strong zonal average component. To make a discussion of this subject manageable, the properties of a variable are first shown when longitudinal averages are taken in additional to seasonal time averages. Longitude averages are commonly labeled “zonal means”. Zonal averages do miss important phenomena that can be seen in time averages. Time means reveal longitudinal variations that one must consider in order to

understand the properties as well as the maintenance of the zonal mean state. The three dimensional structure of time averages is treated by showing horizontal maps of time averaged fields a few representative levels.

The general circulation undergoes seasonal change. In many fields the seasonal change is much less in the Southern Hemisphere than in the Northern Hemisphere. The difference arises because the middle latitudes in the Southern Hemisphere have a much higher fraction of ocean coverage than in the Northern Hemisphere. Land and ocean have different thermodynamic properties: heating and cooling are more readily mixed through a greater amount of mass in the ocean than on land; the albedo of land can change drastically with season unlike ice-free ocean, and water has a higher heat capacity than soil. These factors magnify seasonal change over large land masses.

The difference in middle latitude land coverage has another implication. There are more major mountain ranges in the Northern Hemisphere. The mountains, along with differences that arise between land and sea areas lead to more prominent planetary waves in the Northern Hemisphere. Alternatively, many fields in the Southern Hemisphere tend to be more zonally-uniform.

1.2 RADIATION AND TEMPERATURE

1.2.1 Radiation

A discussion of the general circulation starts with radiation since the distribution of radiation absorbed and emitted is the ultimate driving mechanism for the circulation.

The Earth (including its atmosphere, solid, and ocean parts) absorbs radiation emitted by the sun. While the Earth rotates about an axis that is tilted with respect to the sun, the equator is perpendicular to the sun's rays on an annual average. Simple geometry (see Fig. 1) shows that the solar radiation reaching a unit horizontal area on the Earth diminishes from equator to pole. The amount of solar radiation absorbed is influenced by the reflectivity of the Earth's surface, the amount of cloud cover, and the path length through the atmosphere. On an annual average, the amount of radiation absorbed decreases greatly from the equator towards each pole (Fig. 1). The *rate* that absorption decreases with latitude is greater in polar than in tropical regions.

< FIG. 1 here>

To balance the radiant energy absorbed, the Earth emits energy back to space. Like the absorbed solar radiation, terrestrial emission also decreases from the equator towards each pole on an annual average. The terrestrial emission is governed by the temperature and the radiative properties of the emitter. Emission comes from the surface of the Earth as well as from the atmosphere. For equivalent radiative substances, more radiant energy is emitted from objects having higher temperature. So, the terrestrial emission shown in Fig. 1 is consistent with the tropics being warmer than the polar regions. A key fact is that the emission does not change with latitude nearly as fast as does the absorption. Consequently, most latitudes are not in radiative equilibrium and there is a net radiation surplus in the tropics (more solar radiant energy is absorbed than terrestrial radiation is emitted). Poleward of 38 degrees latitude there is a net radiation deficit (more emission than absorbion locally). In order to sustain the surplus and deficit over time, a poleward energy transport is required, and that has implications for the temperature field. The terrestrial emission means that temperatures are lower in the tropics and warmer in the polar regions than they would be if there was no heat transport. While some transport occurs by the oceans, the remainder occurs in the atmosphere and to transport thermal energy the atmosphere must have a circulation. The atmosphere may transport the heat by direct means (labeled sensible heat transport) or by transporting water vapor (labeled latent heat transport). The latter process gains or releases heat during a phase change of the water. So, the distribution of radiation implies links to temperature, velocity, and moisture fields.

The solar absorption and terrestrial emission shown in Fig. 1 are plotted on a stretched latitudinal scale. The stretching is proportional to the horizontal area of each latitude band. Consequently the annual average energy balance for the earth as a whole is also seen in the figure because the areas under the two dashed curves are the same. More is said about the energy distribution and flow in the chapter on General Circulation Energetics.

While Fig. 1 shows the zonal average distribution of absorbed and emitted radiation, the longitudinal distribution of those two quantities is shown in Fig. 2. The annual average solar radiation absorbed (Fig. 2a) has a strong zonal mean component over the oceans. The principal deviations from the zonal average are over ice-covered regions (Greenland) and desert areas (Sahara and Arabia). Both areas have high annual average reflectance either due to a bright surface. Variation across each ocean basin occurs with greater cloudiness along the storm tracks (discussed below) such that those tracks avoid the eastern sides and allow more solar absorption on the east side. The dips in the zonal average radiant energies near 10 N latitude (Fig.1) are a consequence of

persistent high-elevation cloudiness associated with the intertropical convergence zone (ICZ). The ICZ is seen in Fig. 2a as most of the lower values in the tropics that occur over the major land masses and along a narrower band across the oceans. The annual average terrestrial radiant flux at the top of the atmosphere (Fig. 2b) also has a strong zonal mean component over oceans. Longitudinal variations occur for the eastern subtropical oceans, deserts, and higher topography. The ICZ is visible as lower values of terrestrial radiant fluxes in the tropics because the emission is primarily from the cold tops of high clouds. The same clouds strongly reflect solar radiation causing a corresponding solar radiation pattern. The net radiation (Fig. 2c) has a strong latitudinal trend as deduced from Fig. 1. The primary zonal variations are over the subtropical deserts. These areas are hot (high thermal emission) but reflective (reduced solar absorption) leading to negative net radiation. For thermal balance, energy must be exported from areas of positive to areas of negative net radiation; so the subtropical deserts maintain their high heat in part because heat energy converges into those deserts. Also, the dry desert surface means the solar energy absorbed mainly heats the surface and overlying air but evaporates little water.

<Fig. 2 here>

1.2.2 Temperature

In the troposphere and lower stratosphere, absorption and emission of radiation alters the air temperature at a rate of a few degrees per day. This change of air temperature is generally small compared to the difference between the equatorial regions and the polar regions. Hence, the radiant energy absorption and emission do not create large temperature differences between the daylight and night sides of the Earth. Therefore, much about the atmosphere's thermal structure is seen in a zonal mean.

Seasonal averages for winter and summer temperature are displayed in Fig. 3. These properties are evident in the figure:

<Fig. 3 here>

i. Temperature decreases with increasing height in the troposphere and winter stratosphere. The rate of change with height (equaling minus the lapse rate) is greater in the troposphere and notably less in the stratosphere. The lapse rate is less than the lapse rate for neutral stability; so, the atmosphere is statically stable

on the large scale. Temperature increases with height in the tropical lower stratosphere.

ii. The tropopause marks the boundary between the stratosphere and troposphere. The zonal mean tropopause is not level, but ranges from 6-8 km (~500-350 hPa) in polar regions to 16-18 km (~100-80 hPa) in the tropics.

iii. In the troposphere, zonal mean temperature along an isobaric surface decreases towards each pole. The rate of decrease (the meridional gradient) is small in the tropics. This gradient is larger in the middle latitudes (30-60 degrees latitude). An exception is the sharp gradient near the Antarctic coast. The gradient is stronger during winter. The temperature change from equator to pole is also greater at the surface than in the middle troposphere.

iv. The coldest temperatures are in the winter stratospheric polar region and near the equatorial tropopause.

v. In much of the lower stratosphere, the zonal mean temperature gradient is reversed from the troposphere. The reversal is evident in much of the tropics and middle latitudes. The main exceptions are the higher latitudes and part of the Southern Hemisphere middle latitudes during winter.

The longitudinal distribution of the temperature is illustrated by the 850 hPa level temperatures shown in Fig. 4. As anticipated from the terrestrial radiation data, the field has notable zonal symmetry over the oceans. The colder temperatures in middle latitudes tend to be over the eastern sides of the continents during winter. Large ice-covered regions have colder temperatures. During summer the hottest temperatures are located over the subtropical deserts.

<Fig. 4 here>

1.3 MASS FIELDS

1.3.1 Geopotential height fields

The temperature field is related to the mass fields in several ways. For example, the hypsometric equation demonstrates that the spacing between isobaric surfaces is proportional to the mean virtual temperature of the air between those surfaces. In the troposphere, the vertical distance between any two isobaric surfaces (the “thickness”) is

larger in the tropics than outside the tropics. Since the variation of sea level pressure over the globe is rather small, this implies that the altitude of an upper air constant pressure surface (500 hPa, say) on average increases from pole to equator.

The zonal and time mean geopotential heights of the 500 and 1000 hPa geopotential height surfaces (Z_{500} and Z_{1000}, respectively) are shown in Fig. 5 for the two extreme seasons. The Z_{500} surface is representative of geopotential height surfaces in much of the troposphere and lower stratosphere. At 500 hPa, higher heights are found in the tropical regions with lowest values near the poles. The gradient between equator and pole is strongest in the middle latitudes and during winter. The Z_{1000} pattern is representative of the mass field near the surface. The zonal average Z_{1000} has lower values near the equator, with higher values in the subtropics (more so in local winter). The lower values in middle latitudes are associated with the midlatitude storm tracks.

<Fig. 5 here>

1.3.2 Midlatitude Planetary Waves and Storm Tracks

The mass and temperature fields have significant longitudinal variation. Away from the surface, the time mean pattern is characterized by long waves. The time mean Z_{500} (Fig. 6) has patterns typical of much of the troposphere. Prominent troughs are seen near the midlatitude east coasts of Asia and North America. The temperature field beneath (e.g. Fig. 4) also has colder values (thermal troughs) near these regions. A weaker geopotential trough occurs over the Mediterranean and northwest Africa. At the base of each trough the height contours are more closely spaced; from geostrophic wind balance one expects the wind speeds to be relatively stronger there. Ridges are found in between, most prominently in northwestern North America and Europe. In summer, the North American trough remains visible due to the cold air over the Baffin and Greenland ice sheets.

Consistent with the zonal average distribution (Fig. 5) the time average gradient is strongest in middle latitudes. While the gradient has similar strength during winter, during summer the time mean gradient is stronger in the Southern Hemisphere.
<Fig. 6>

Most of the weather in the middle latitudes is created by the travelling frontal cyclones, otherwise known as extratropical cyclones. These cyclones interact with the planetary wave pattern in various ways. These cyclones prefer to form, propagate and decay in specific regions. Generally speaking, frontal cyclogenesis is favored in three types of regions: near the east coasts of continents, on the lee side of major mountain ranges, and where large-scale surface temperature gradients are strong. Most of these

regions coincide with the long wave trough locations. A region of stronger sea surface temperature gradient lies South of Africa and across much of the southern Indian Ocean. Further south, the near the surface temperature gradient is intensified at the edge of Antarctic sea ice. The frontal cyclones generally progress eastward and poleward as they evolve. Fig. 6 also shows various archetypal tracks followed by many frontal cyclones. Individual tracks of cyclones vary, but the thicker dashed arrows in Fig. 6 indicate the more common paths. In the Northern Hemisphere cyclones often merge with or supplant the "semi-permanent" Aleutian and Icelandic lows that are visible in the sea level pressure field discussed next. The storm tracks show up in the precipitation fields (shown later) as bands of heavier precipitation in the middle latitudes across the oceans. Precipitation also is enhanced where westerlies encounter mountain ranges of North America and western Europe.

1.3.3 Sea level pressure and Subtropical Highs

The sea level pressure (SLP) pattern (Fig. 7) differs from the mass field pattern at mid and upper troposphere levels (e.g. the Z_{500} pattern of Fig. 6). An obvious difference is that the field is noisy over major topographic features because it is based on extrapolating the pressure to sea level. Another difference is the meridional height gradient (created by the meridional temperature gradient through a depth of the atmosphere) is not so evident at the surface. So, the SLP pattern is more cellular. Another difference is that colder air aloft can result in relatively higher surface pressure near the ground (due to higher average density of the air above compared to an adjacent region). The converse is also true for lower pressure where the air aloft is warmer than the surroundings (so called 'thermal lows'). This relationship is the opposite to that described above for upper air geopotential height because the hypsometric equation relates to the thickness of a layer, not the bottom of a layer.

<Fig. 7>

At the surface one finds prominent high pressure cells in the subtropics. These cells generally prefer the eastern sides of the ocean basins where thermal and other forcing builds higher pressure. For example, equatorward winds on the east side of the subtropical high can drive upwelling of colder subsurface ocean water and the resultant cooler surface is observed to lead strengthening of the high (a result also consistent with potential vorticity reasoning). The colder temperatures foster low stratus clouds which in turn create a net radiative cooling of the air and additional forcing for the high. The areal extent of the highs is influenced by other factors such as the midlatitude storm tracks and tropical convection. In summer, these factors allow much greater expansion of the

subtropical highs in the Northern than in the Southern Hemisphere. A three-way balance between the pressure gradient, Coriolis, and turbulent drag forces implies divergence at a surface high. Surface divergence is consistent with the sinking and eastern sides of the subtropical highs can be viewed as regions where the sinking branch of a Hadley cell is enhanced. The sinking is apparent as areas where upper level divergent winds converge (shown below). The tropical convection, mainly equatorward and to the west of the subtropical high, feeds the circulation supporting the high; this link is visible in the divergent winds.

1.4 WIND FIELDS

1.4.1 Zonal Velocity

The zonal wind is directed positive when blowing towards the east. Outside the equatorial region, the mass and wind fields are in approximate geostrophic balance. The meridional gradient seen in the tropospheric geopotential height fields implies a westerly wind which is stronger in middle latitudes. At the surface, comparatively weak winds are expected.

The thermal wind relation states that vertical *shear* of the zonal wind is proportional to the meridional gradient of temperature and inversely proportional to the Coriolis parameter. The temperature gradient in much of the troposphere is directed equatorward, an orientation implying westerly wind shear. Since the tropospheric temperature gradient is stronger in middle latitudes, one expects the westerly shear to be stronger there as well. The temperature gradient reverses in the tropical and middle latitudes of the lower stratosphere implying easterly shear. Therefore, one anticipates westerly winds to increase with height in the troposphere and to decrease above, in the lower stratosphere. In short, the stronger westerly winds tend to occur at tropopause level.

Another constraint on the zonal wind is angular momentum balance. If the winds at the surface were everywhere westerly (say) then those winds would apply a net torque upon the surface of the Earth. A net westerly torque would speed up the rotation of the Earth and the days would be getting shorter. However, the angular momentum of the Earth is essentially constant. So, one expects that areas of easterly winds are balanced by areas of westerly winds at the surface.

The zonal mean of the zonal wind is shown in Fig. 8 for winter and summer. Areas that are shaded indicate easterly winds. These properties are evident in the figure.
<Fig. 8>

i. The surface winds are generally easterly in the tropics which cover approximately half of the surface area of the globe. The surface winds are primarily westerly in the middle latitudes.

ii. The winds generally gain a westerly component with elevation. For the tropical troposphere, the easterly wind decreases with increasing elevation. For much of the middle latitudes, the westerly wind increases with height until the tropopause. Above, the vertical shear reverses and the westerlies decrease with increasing height. The principal exceptions are the high latitudes in winter. These properties, including the exceptions, are anticipated from the temperature gradients shown above (Fig. 3).

iii. In the high latitude, winter stratosphere, westerly winds increase with height. It is difficult to see with the vertical coordinate chosen, but these westerly winds are associated with the polar night jet. That jet reaches maximum speed in the upper stratosphere (10-30 hPa level).

iv. The subtropical jets are prominent maxima at the midlatitude tropopause. These jets are stronger and migrate to a lower latitude in winter. In the Southern Hemisphere during winter, strong winds of the polar night jet extend into the troposphere creating the impression that there are two tropospheric jets on upper level isobaric charts. During northern summer an easterly jet is visible at tropopause level just north of the equator.

1.4.2 Meridional Circulations

The meridional wind at a specific location can often be comparable in magnitude to the zonal wind. However, if the meridional wind is geostrophic, then a zonal average of the meridional wind is the integral (with respect to longitude) of a longitudinal derivative. Unless a mountain intercepts the integral path, this integral must be zero because the integral completes a circuit. Since the total wind is nearly in geostrophic balance outside the tropics, the zonal mean meridional wind is very small outside the tropics.

Since the observed lapse rate is less than the dry adiabatic lapse rate, it follows that vertical motions are resisted. One consequence is that vertical motions are far smaller in magnitude than are horizontal motions on this large scale. Large-scale vertical motion

cannot be directly measured since it is smaller than the errors of the observing systems. Vertical velocity can be estimated indirectly from quantities that are measured with some confidence. One procedure is to merge measured meridional winds in the tropics with meridional winds elsewhere estimated from an equation for angular momentum balance and then deduce a stream function in the meridional plane. An alternative procedure is to input observed fields into a primitive equation general circulation model and let the model deduce the vertical motion. The latter procedure obtained the motions shown in Fig. 9.

<Fig. 9>

The zonal mean motions in the meridional plane have these properties:

i. The motion is organized into distinct patterns commonly referred to as meridional cells. The most prominent cells occur in the tropics and are often named the “Hadley” cells. In the middle latitudes of each hemisphere is found a much weaker circulation usually labeled the “Ferrel” cell.

ii. The meridional cells are much stronger during winter both in terms of the areal extent they occupy as well as the vigor of the circulation. The winter Hadley cell has significant flow across the equator.

iii. In the Hadley cell, air circulates in an intuitive sense: rising motion occurs where the mean temperature through the depth of the atmosphere is warmer, sinking motion where it is cooler. The temperature distribution over the globe is statically stable in the dry sense. However, in the lower tropical troposphere the air is very moist and nearly neutral with respect to a psuedoadiabatic lapse rate. The upward motion of the Hadley cell is driven by latent heat release as water vapor is converted into precipitation. So, one expects precipitation to be a maximum in the tropics. In order to overcome the moist static stability and entrainment as air parcels rise into the upper tropical troposphere, the rising motion is embedded within thunderstorms. These thunderstorms occupy a very small fraction (about 0.5 %) of the tropical surface area. Air parcels in the poleward moving branch of the Hadley cell cool radiatively; as their potential temperature decreases these parcels sink.

iv. In the Ferrel cell, air appears to rise where temperatures are cooler and sink where they are warmer. This Eulerian mean motion should not be confused with the actual paths of air parcels. In middle latitudes parcel motions are strongly influenced by baroclinic waves. The zonally-varying (eddy) flow associated with baroclinic waves has comparable meridional and zonal components. When an average is taken around a latitude circle at constant pressure, the northward and southward motions nearly cancel and the resulting mean has the sense given by the Ferrel cell. Such a mean creates a misleading picture of the motions of air parcels. However, if an average is taken along constant entropy surfaces, the resulting zonal mean in isentropic coordinates shows a meridional circulation having rising in the subtropics and sinking at high latitudes, i.e. the same sense as the Hadley circulation.

The pattern in isentropic coordinates follows from the mass distribution of baroclinic eddies: in an upper isentropic layer slightly more mass is heading polewards than equatorwards; vice versa for a lower layer. Therefore, in isentropic coordinates the motion is more intuitive: rising motion at lower latitudes and sinking motion at higher latitudes. Even though the Ferrel cell does not reflect the actual motion of parcels, the Ferrel cell does depict components of the motion necessary to counteract eddy fluxes of heat and momentum that would otherwise destroy thermal wind balance. (Eddy heat fluxes reduce the meridional temperature gradient while eddy momentum fluxes increase the westerly vertical shear. Planetary angular momentum and vertical adiabatic heat transports by the Ferrel cell can counteract these eddy fluxes.)

v. The radiative energy distribution requires a meridional circulation to transport heat poleward. The meridional motions of the Hadley cell transport the same mass poleward as southward (ignoring the mass due to moisture). The Hadley cell has a net heat transport because the upper level air has higher moist static energy than does the lower level air. In the case of the Ferrel cell, the frontal systems have strong heat fluxes that can be deduced from westward tilts with height of the trough and ridge axes of these waves.

1.4.3 Divergent Tropical Circulations

<Fig. 10>

The Hadley cell upward motion is part of the divergent winds of the tropics. Diverging arrows in Fig. 10 imply rising motion below. Following the divergent wind vectors appears to connect areas of preferred rising with the sinking above the eastern sides of several subtropical highs. Some divergent winds are poleward and thus consistent with the Hadley circulation at 200 hPa. The strongest areas of divergence in Fig. 10 overlie Southeast Asia, Indonesia, and Amazonia. In northern summer, the Southeast Asian Monsoon is prominent. The figure also shows prominent east-west motion in the Pacific that is generally referred to as the "Walker" circulation. The Walker circulation apparently connects rising motion (and thus precipitation) over the far western Pacific with enhanced sinking over the east side of the subtropical high in the eastern Pacifc. The rising air is fed by low level convergence and that results from ageostrophic motions that occur for relatively low surface pressure (Fig. 7B). Low pass filtered observations show a correlation between heavier precipitation in Indonesia, lower pressure there, and stronger Pacific subtropical highs.

1.4.4 Subtropical Jet Streams

Zonal variations of the subtropical jet streams are linked to several phenomena discussed above. The time mean wind speed is plotted in Fig. 11. Consistent with geostrophic balance, the winds are stronger where the horizontal gradient of time mean geopotential height is stronger. That gradient was stronger at the bases of long wave troughs in geopotential (and temperature) near the east coasts of Asia, North America and Australia (during local winter).
<Fig. 11>

The Northern Hemisphere subtropical jet streams has a larger relative maxima near the east coast of Asia than the corresponding part of North America. These maxima are much stronger during winter (DJF). The downstream end of each of these maxima is further poleward than the upstream end. Consequently, two jets occur over both the eastern Pacific and the eastern Atlantic; one velocity maximum south of the other. This combination of velocity maxima contributes to sinking above the east side of the SLP subtropical highs.

In the Southern Hemisphere the jet streams are more zonally-oriented. In summer there is a tendency for stronger flow south of Africa. In winter (JJA) the stronger winds occur east of Australia. As anticipated from the zonal mean (Fig. 8) there is a secondary maximum at a higher latitude (in the southern Indian Ocean and south of New Zealand).

The more southerly maxima are a downward expression of the stratospheric polar night jet.

The divergent winds of the Hadley cell advect planetary angular momentum poleward and thereby strengthen the subtropical jets. As shown in Fig. 10, the tropical circulation is not uniform with longitude but rising motion is enhanced in certain regions. The poleward motion consequently strengthens the subtropical jet in favored locations. Near the east coast of Asia, divergent winds blowing northward from the Indonesia region during northern winter builds higher pressure to the southeast of the Asian long wave trough. The higher pressure there amplifies the height gradient on the southeast side of that trough making the jet is stronger. The divergent flow southward from the Indonesia region contributes to the stronger jet over Australia by similar reasoning.

1.5 MOISTURE

1.5.1 Clouds

Fig. 12 shows the distribution of clouds in terms of cloud amount. Cloud amount is a measure of the fractional area of the sky covered by clouds. Fig. 12 shows the total cloud and the cloud amounts in three ranges based on an estimate of the pressure at the top of each cloud. Clouds at one location often occur at multiple levels, however satellites observe the topmost layer. Since satellites observe the highest clouds, the seasonal means of the middle and low clouds shown in Fig. 12 have been augmented by other observations of humidity beneath higher clouds over some land areas.
<Fig. 12>

Areas of rising motion deduced from the velocity potential (Fig. 10) are co-located with some, but not all of the cloudy regions. The broad regions of rising motion deduced from Fig. 10 correspond with generally smaller cloudy regions with some details in the cloud structure related to the topography. Generally the match between Figs. 10 and 12 is better for deep clouds (areas having higher cloud amounts at all levels). Some areas of sinking deduced from the velocity potential over the eastern ocean basins are also near persistent clouds, but these are low clouds.

The following properties are evident in the seasonal mean cloud amounts:

i. Deep clouds are found along the ICZ. The clouds tend to occupy a narrower band over the oceans (e.g. the Eastern Pacific) and are broader over the large tropical land masses (e.g. Southeast Asia). The impact of the ICZ cloudiness on radiation was noted in Fig. 2.

ii. Cloud amounts are low over subtropical deserts but high over the adjacent east sides of the subtropical oceans. These clouds are confined to low elevation and tend to be more prominent during local spring (Southern Hemisphere) or summer (Northern Hemisphere).

iii. Cloud amounts are high along the midlatitude storm tracks (Fig. 6). In the Northern Hemisphere, the high and middle levels cloudiness along the storm tracks is notably greater during winter. The corresponding seasonal change in the Southern Hemisphere is less obvious.

1.5.2 Precipitation

Precipitation is linked to the general circulation in several ways. Fig. 13 shows the zonal mean distribution of precipitation rate. The largest precipitation rate occurs in the tropics along the ICZ and is associated with the rising branch of the Hadley cells. The peak value migrates to about 10 to 15 degrees latitude in the summer hemisphere (on a zonal average); a migration consistent with the dominance of the winter hemisphere Hadley cell (Fig. 9). In some seasons, two equatorial maxima are found whose explanation becomes clear when time mean fields are consulted. Subtropical sinking motion seen in the meridional cells suppresses the precipitation rate. Secondary maxima occur in middle latitudes that are superficially linked to the rising branch of the Ferrel cells, but are more properly associated with the extratropical cyclones. While the cloudiness (Fig. 12) is high in high latitudes, the colder air does not contain as much water vapor mass as in the tropics.
<Fig. 13>

The zonal mean Hadley circulation implies transport of moisture from the subtropics towards the ICZ. The vigorous upward motion near the equator and that motion is driven by precipitation formed within thunderstorms that cover only a small fraction of the tropics at any one time. The time mean precipitation, Fig. 14, shows tropical precipitation matching the larger cloud masses (especially high cloud) shown in

Fig. 12. Therefore, precipitation rate is higher over tropical land areas and regions of warmest sea surface temperature (i.e. western Pacific). During southern summer, precipitation is greatly enhanced over the southern Indian Ocean and tropical land masses, while over the eastern Pacific the ICZ remains north of the equator resulting in the double maximum seen in the zonal average during DJF (Fig. 13). The South Pacific Convergence Zone is also prominent; part forms the ICZ of the western Pacific and part is northwest-southeast oriented line of higher precipitation across the South Pacific.

Higher time mean precipitation rates (Fig. 14) are found along the midlatitude storm tracks (Fig. 6) with larger amounts near the start of the tracks and where the flow encounters topography (west coasts of the Americas).

<Fig. 14>

1.6 BROAD SUMMARY

The observed time and zonal mean properties of the large scale primary atmospheric variables were briefly described. Above the planetary boundary layer, these variables tend to have stronger meridional than longitudinal variation, thereby validating the use of zonal average depictions. The zonal variations are related surface properties (land versus sea, ice versus vegetation, surface temperature gradient) and major topographic features. Seasonal changes were described; the most general comment is seasonal variation is less in the Southern compared with the Northern Hemisphere.

1.7 FURTHER READING

Grotjahn, R. (1993) Global atmospheric circulations: Observations and theories. New York: Oxford University Press.

Grotjahn, R. (2008) Different data, different general circulations? A comparison of selected fields in NCEP/DOE AMIP-II and ECMWF ERA-40 reanalyses. Dynamics of Atmospheres and Oceans 44, 108-142.

James, I. N. (1994) Introduction to Circulating Atmospheres. Cambridge: Cambridge University Press.

Johnson, D. R. (1989) The forcing and maintenance of global monsoonal circulations: An isentropic analysis. In: Advances in Geophysics, 31, 43-316. San Diego: Academic Press.

Karoly, D. J. and Vincent, D. G. (1998) Meteorology of the Southern Hemisphere. Boston: American Meteorological Society.

Peixoto, J. P. and Oort, A. H. (1992) Physics of climate. New York: American Institute of Physics.

Schneider, T., Sobel, A. H. (2007) The Global Circulation of the Atmosphere. Princeton: Princeton University Press.

(suggested cross-references)

See also: Dynamic meteorology, General circulation overview, General circulation energy cycle, General circulation: momentum budget, General circulation models, Hadley circulation, Jet streams, Middle atmosphere zonal mean climatology, Monsoon overview, Planetary atmospheres, Radiation budget: planetary, Synoptic meteorology: weather maps, Tropical meteorology: tropical climates, Walker circulation, Global change: upper atmosphere change, Climate variability: seasonal and interannual variability.

FIGURE CAPTIONS

Figure 1 Schematic diagram of solar radiation reaching two horizontal areas on the Earth at an equinox. Inset: latitudinal distribution of incoming solar (dotted line), absorbed solar (short dashed line), and terrestrial emission (solid line) in W m^{-2}. A stretched latitude is used based on the area within each latitude band. Data from NCEP/DOE AMIP Reanalysis II four times daily mean data averaged from January 1979 through December 2009.

Figure 2 Annual radiative balance for the Earth. (A) Time average incoming, downward, solar, absorbed radiation estimated at the top of the atmosphere. (B) Time average upwelling, longwave radiation from the Earth. (C) Net radiation, the solar minus terrestrial radiation

difference. NCEP/DOE AMIP Reanalysis II four times daily mean data averaged from January 1979 through December 2009. Contour interval 20 W m^{-2}.

Figure 3 Zonal mean temperature during (A) December–February and (B) June–August. Units are degrees Celsius. The data are from the National Center for Environmental Prediction/National Center for Atmospheric Research (NCEP/NCAR) reanalysis period 1979–99. Contour interval 10 C.

Figure 4 Temperature at 850 hPa in the two extreme seasons. Units are degrees Kelvin. The data are from the European Centre for Medium-range Weather Forecasts ERA-40 reanalysis averaged 1979-2002. Contour interval 5 K.

Figure 5 Zonal mean geopotential heights in (A) at 500 hPa and in (B) at 1000 hPa. Solid line is for December–February seasonal average and dotted line is for June–August. These NCEP/NCAR reanalysis data are from 1979–99.

Figure 6 Geopotential height of the 500 hPa surface (contours) in the two extreme seasons. Units are m. The data are from the European Centre for Medium-range Weather Forecasts ERA-40 reanalysis averaged 1979-2000. Also plotted are general indicators of the frontal cyclone storm tracks (dashed arrows) where a wider arrow indicates more frontal cyclone passages than for a thinner arrow. Frontal cyclone storm tracks shown merge information in van Loon (1966) Geographical Review 56: 497-515; Whitaker and Horn (1984) Journal of Climatology 4: 297–310; Simmonds and Murray (1999) Weather and Forecasting 14: 878–891; Hoskins and Hodges (2002) Journal of the Atmospheric Sciences 59: 1041-1061; Hoskins and Hodges (2005) Journal of Climate 18: 4108-4129; and Dos Santos Mesquita (2008) Tellus 60A: 557-569.

Figure 7 Sea level pressure (SLP) contours in the two extreme seasons. Units are hPa. Contours use 4hPa interval. The data are from the European Centre for Medium-range Weather Forecasts ERA-interim reanalysis averaged 1989-2010.

Figure 8 Zonal mean zonal wind (solid contours; in m s^{-1}) with potential temperature (dashed contours; in K) for seasonal averages (A) December–February and (B) June–August. Areas of easterly winds are shaded. NCEP/NCAR reanalysis data 1979–99.

Figure 9 Zonal mean meridional circulations for (A) December–February and (B) June–August. Some of the large vectors for p > 700 hPa over Antarctica may not be meaningful. Vectors based upon NCEP/NCAR reanalysis data 1979–99.

Figure 10 Time mean divergent wind (arrows) and velocity potential (contours) at 200 mbar during (A) December–February and (B) June–August. The longest arrow is approximately 10m s^{-1} and the contour interval is $2x10^6$ m^2 s^{-1}. NCEP/NCAR reanalysis data 1979–99.

Figure 11 Time mean horizontal wind at 200 hPa for (A) December–February and (B) June–August. Contour interval is 5 m s^{-1}. NCEP/NCAR reanalysis data 1979–99.

Figure 12 Cloud amount during December-February (left column) and June-August (right column). (A) and (E) Total amount at all levels. Estimates of average cloud amounts assigned to three general elevation ranges are also shown. (B) and (F) High clouds in the range 50-440 hPa. (C) and (G) Middle tropospheric clouds in the range of 440-680 hPa. (D) and (H) low level clouds below 680 hPa pressure surface elevation. Cloud amounts based on satellite estimates of the fraction of 5km wide pixels report cloud in each 280 km wide region. Geostationary and polar orbiting satellite data used, leading to some artificial boundary effects (e.g. Indian Ocean). Data are provided by the International Satellite Cloud Climatology Project (ISCCP) D2 monthly means combined from the July 1983 through June 2008 time period. If reproduced in grayscale, dark gray from few clouds, lightest gray for a middle amount of clouds for each indicated range, light inside darker gray for higher amounts in the range. Data maintained by the ISCCP research group at the NASA Goddard Institute for Space Studies, New York, NY. on January, 2005. Rossow, W.B., and Schiffer, R.A., 1999: Advances in Understanding Clouds from ISCCP. Bull. Amer. Meteor. Soc., 80, 2261-2288.

Figure 13 Zonal mean precipitation rate in mm/day for December – February (solid line) and June – August (dotted line). Climate Prediction Center Merged Analysis of Precipitation (CMAP) 1979–99 data used. Data provided by the NOAA/OAR/ESRL PSD, Boulder, Colorado, USA, from their Web site at http://www.esrl.noaa.gov/psd/.

Figure 14 Seasonal time mean precipitation rate for (A) December–February and (B) June–August. Contour interval is 2 mm/day with areas exceeding 10 mm/day shaded. CMAP data 1979-99.

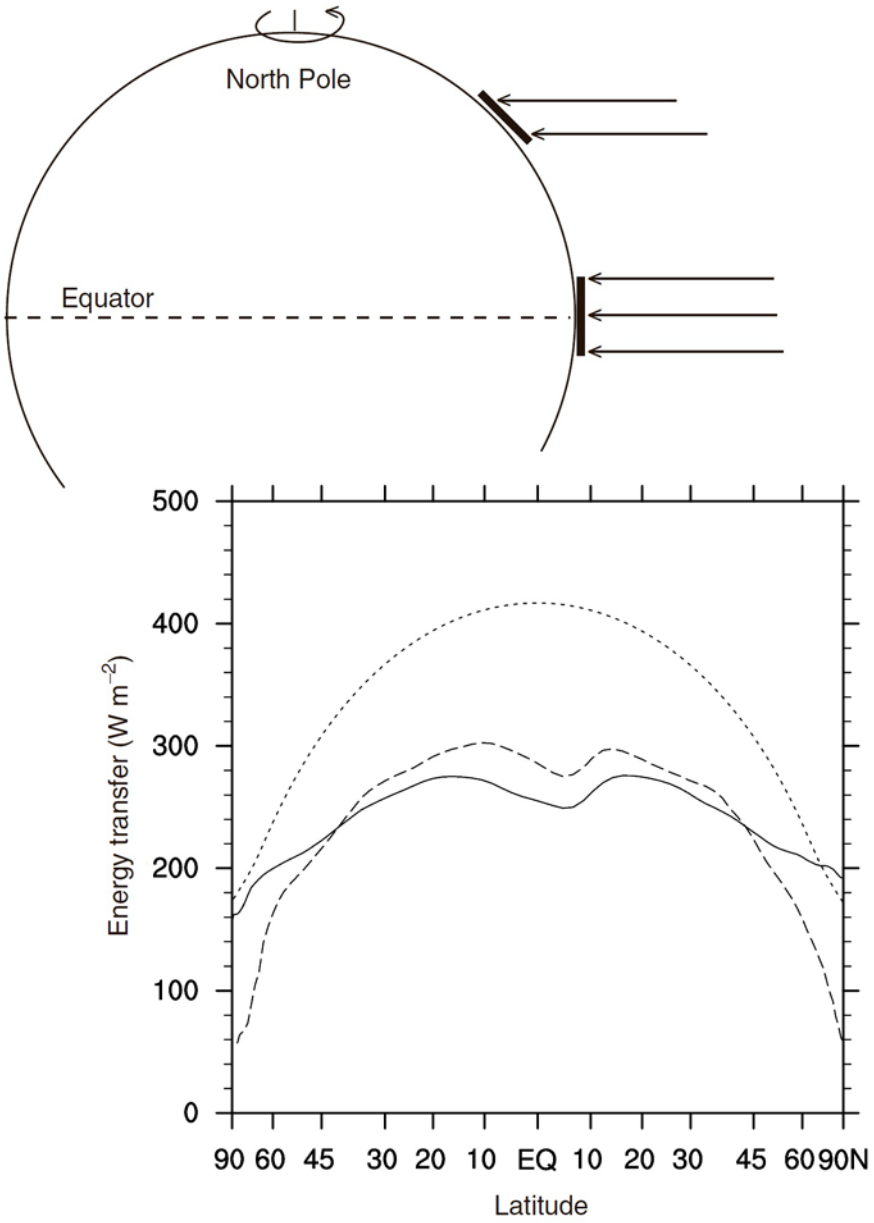

Figure 1 Schematic diagram of solar radiation reaching two horizontal areas on the Earth at an equinox. Inset: latitudinal distribution of incoming solar (dotted line), absorbed solar (short dashed line), and terrestrial emission (solid line) in W m^{-2}. A stretched latitude is used based on the area within each latitude band. Data from NCEP/DOE AMIP Reanalysis II four times daily mean data averaged from January 1979 through December 2009.

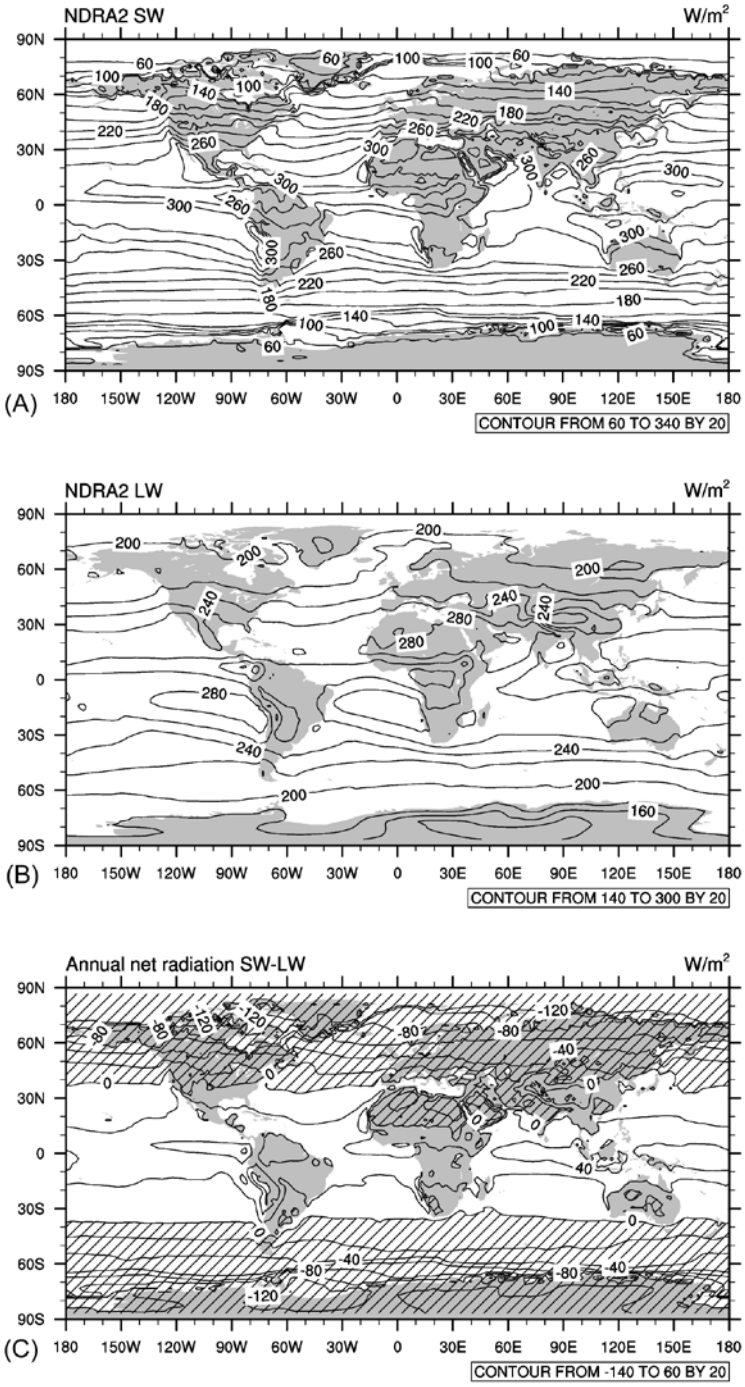

Figure 2 Annual radiative balance for the Earth. (A) Time average incoming, downward, solar, absorbed radiation estimated at the top of the atmosphere. (B) Time average upwelling, longwave radiation from the Earth. (C) Net radiation, the solar minus terrestrial radiation difference. NCEP/DOE AMIP Reanalysis II four times daily mean data averaged from January 1979 through December 2009. Contour interval 20 W m^{-2}.

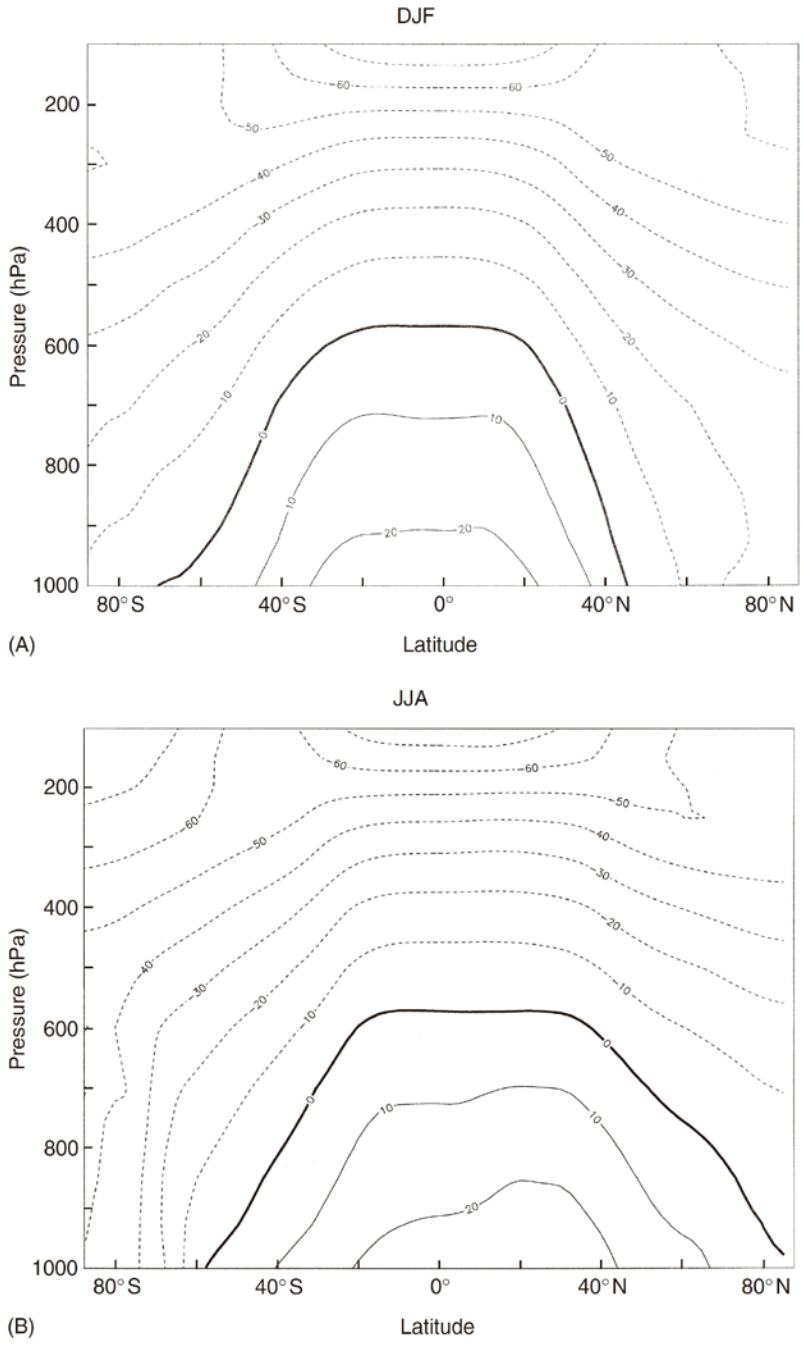

Figure 3 Zonal mean temperature during (A) December–February and (B) June–August. Units are degrees Celsius. The data are from the National Center for Environmental Prediction/National Center for Atmospheric Research (NCEP/NCAR) reanalysis period 1979–99. Contour interval 10 C.

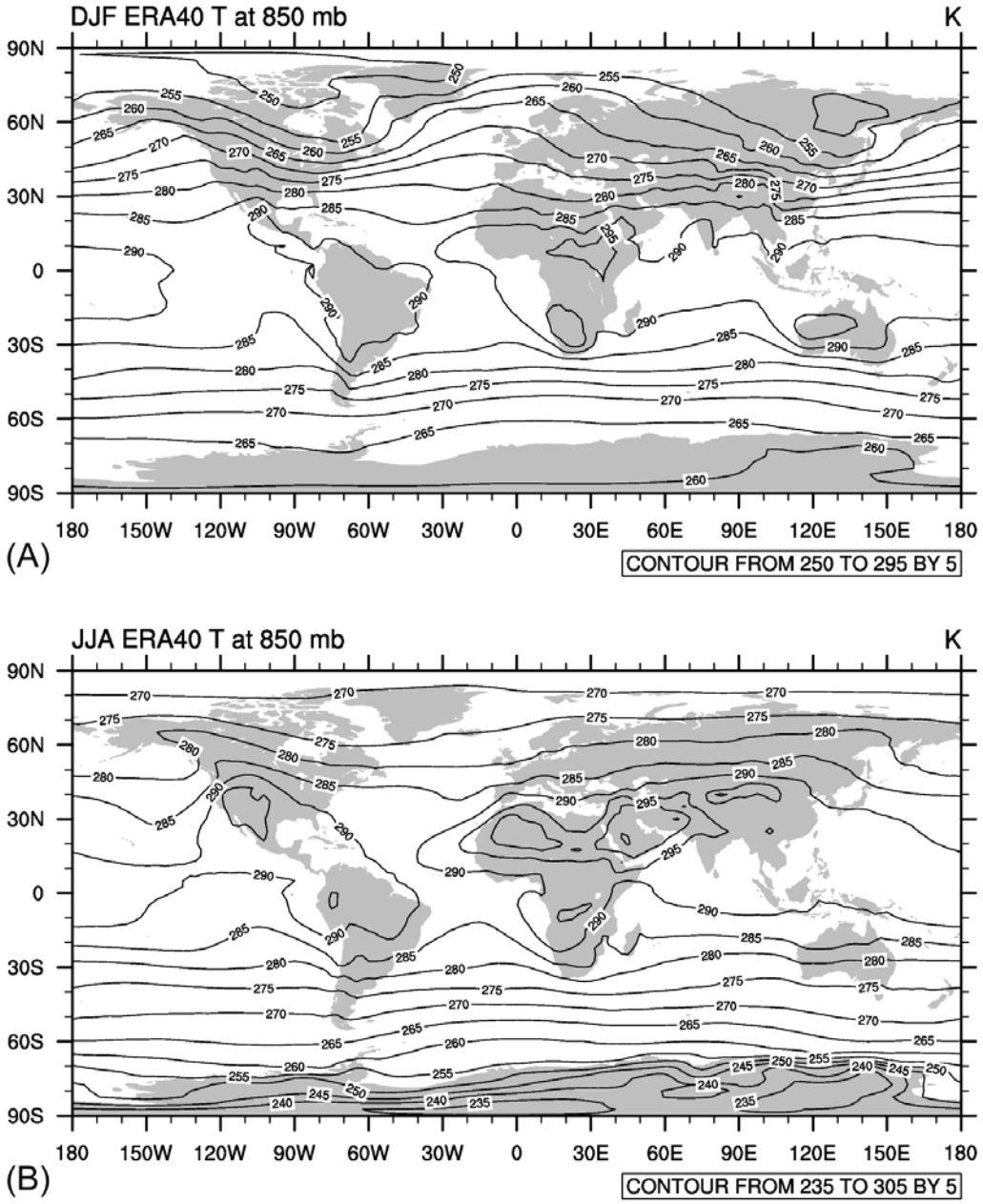

Figure 4 Temperature at 850 hPa in the two extreme seasons. Units are degrees Kelvin. The data are from the European Centre for Medium-range Weather Forecasts ERA-40 reanalysis averaged 1979-2002. Contour interval 5 K.

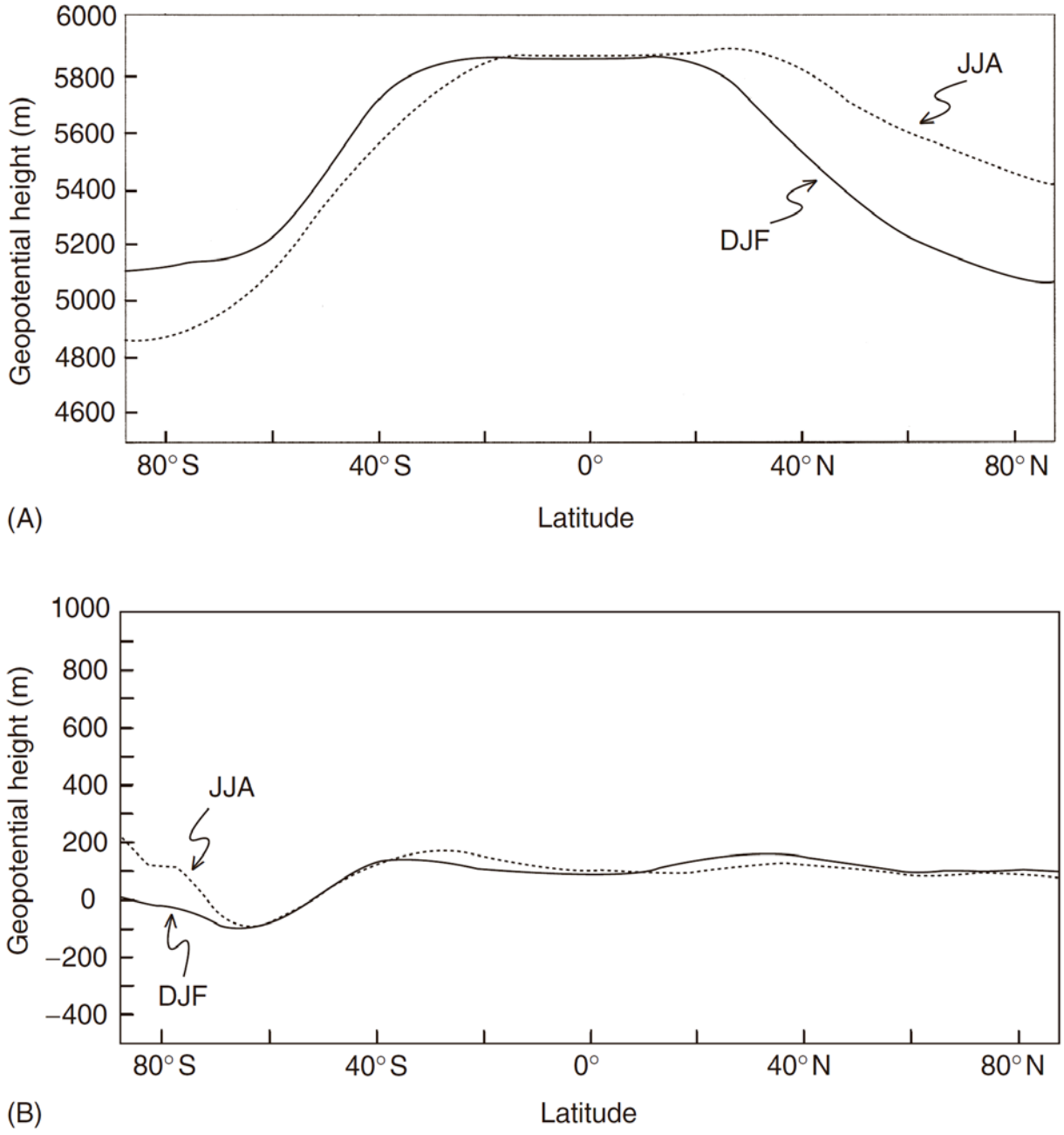

Figure 5 Zonal mean geopotential heights in (A) at 500 hPa and in (B) at 1000 hPa. Solid line is for December–February seasonal average and dotted line is for June–August. These NCEP/NCAR reanalysis data are from 1979–99.

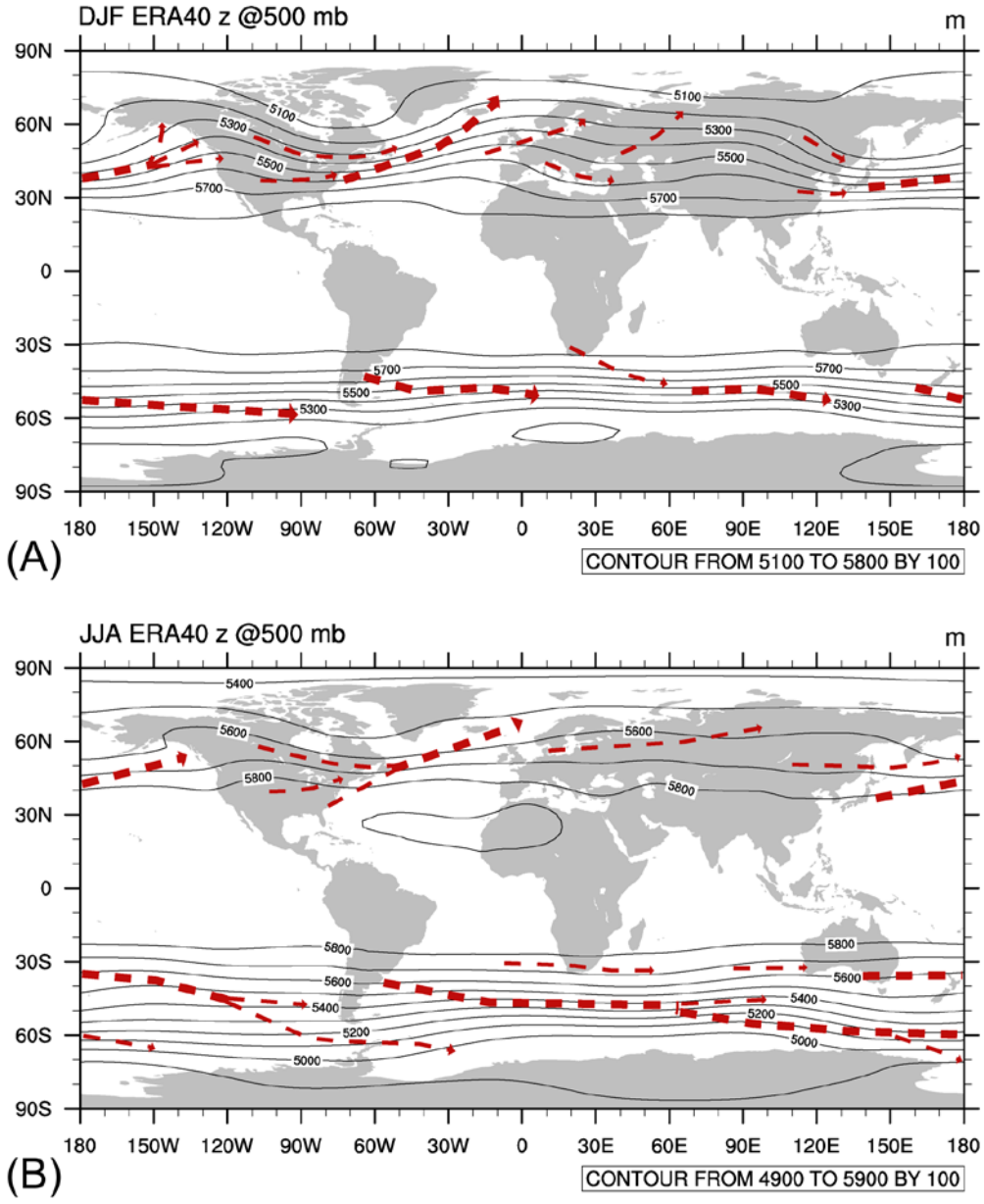

Figure 6 Geopotential height of the 500 hPa surface (contours) in the two extreme seasons. Units are m. The data are from the European Centre for Medium-range Weather Forecasts ERA-40 reanalysis averaged 1979-2000. Also plotted are general indicators of the frontal cyclone storm tracks (dashed arrows) where a wider arrow indicates more frontal cyclone passages than for a thinner arrow. Frontal cyclone storm tracks shown merge information in van Loon (1966) Geographical Review 56: 497-515; Whitaker and Horn (1984) Journal of Climatology 4: 297–310; Simmonds and Murray (1999) Weather and Forecasting 14: 878–891; Hoskins and Hodges (2002) Journal of the Atmospheric Sciences 59: 1041-1061; Hoskins and Hodges (2005) Journal of Climate 18: 4108-4129; and Dos Santos Mesquita (2008) Tellus 60A: 557-569.

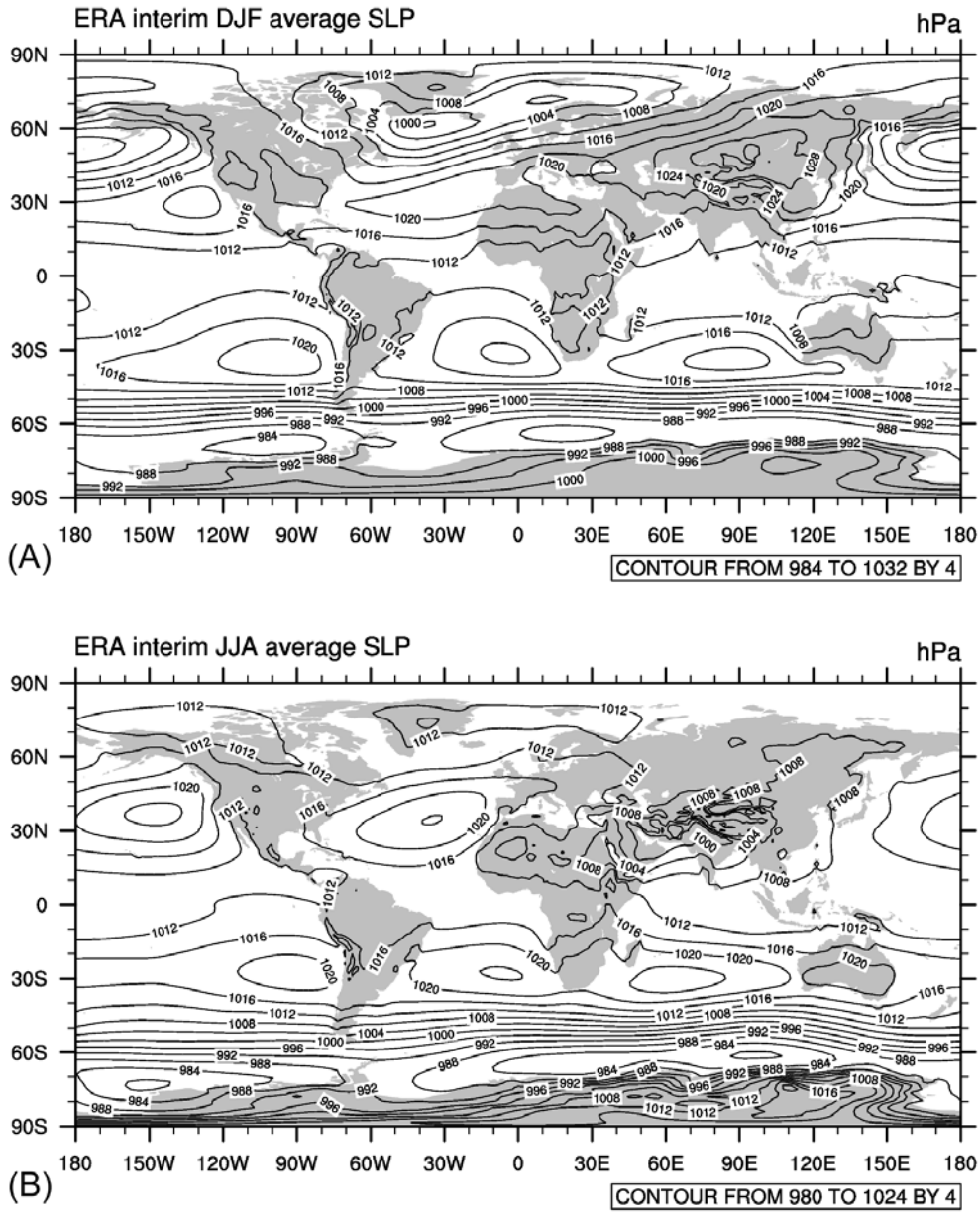

Figure 7 Sea level pressure (SLP) contours in the two extreme seasons. Units are hPa. Contours use 4hPa interval. The data are from the European Centre for Medium-range Weather Forecasts ERA-interim reanalysis averaged 1989-2010.

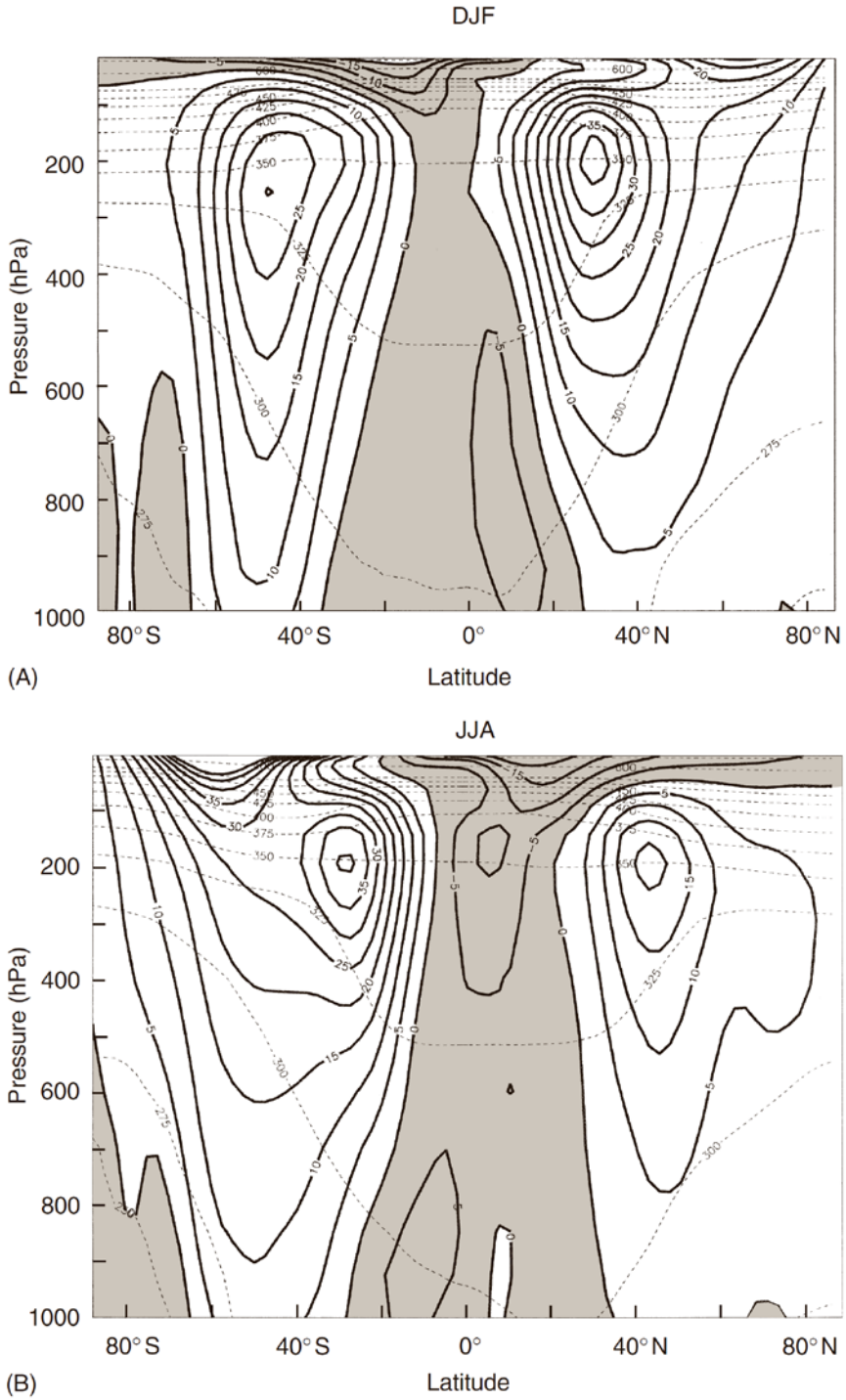

Figure 8 Zonal mean zonal wind (solid contours; in m s^{-1}) with potential temperature (dashed contours; in K) for seasonal averages (A) December–February and (B) June–August. Areas of easterly winds are shaded. NCEP/NCAR reanalysis data 1979–99.

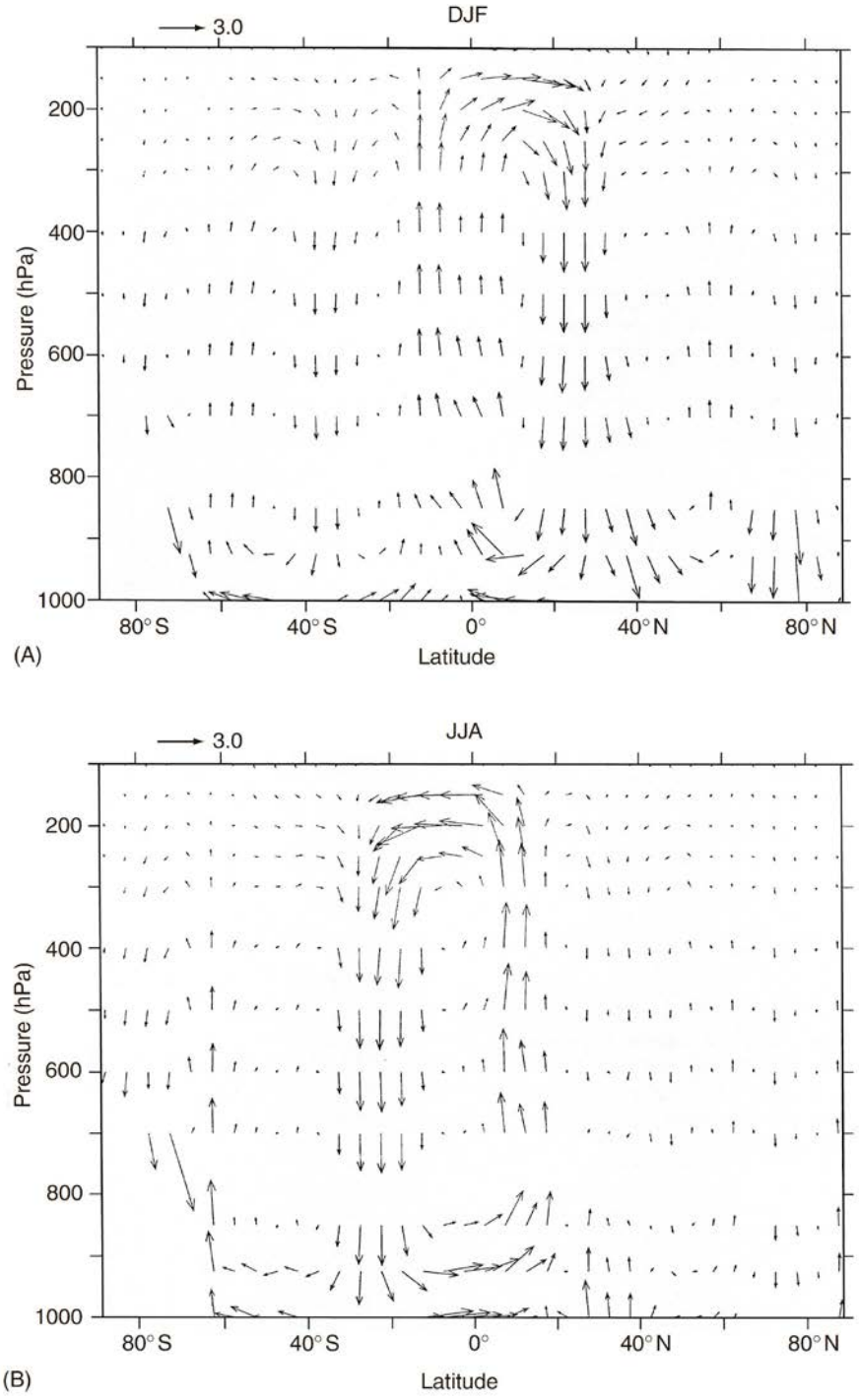

Figure 9 Zonal mean meridional circulations for (A) December–February and (B) June–August. Some of the large vectors for p > 700 hPa over Antarctica may not be meaningful. Vectors based upon NCEP/NCAR reanalysis data 1979–99.

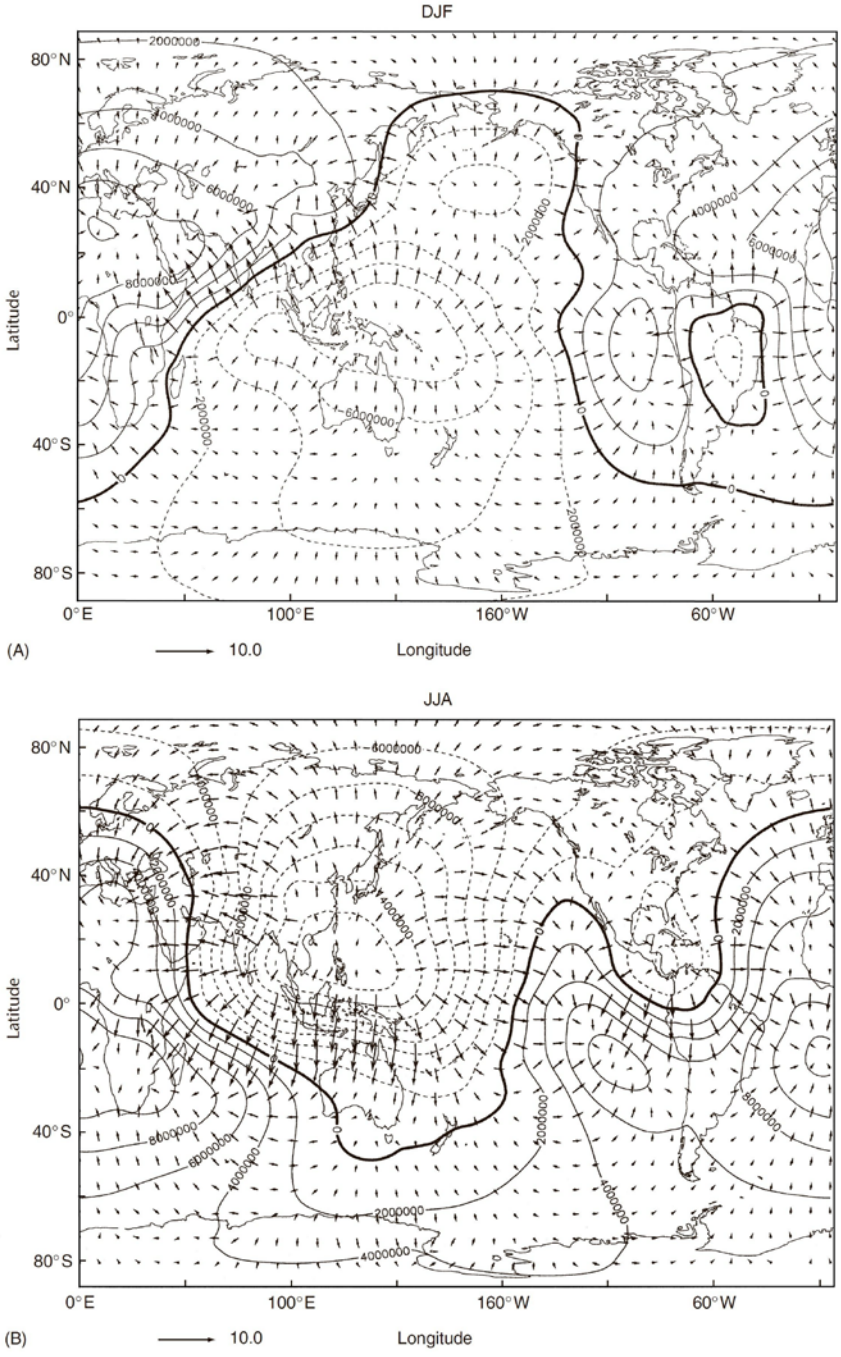

Figure 10 Time mean divergent wind (arrows) and velocity potential (contours) at 200 mbar during (A) December–February and (B) June–August. The longest arrow is approximately 10m s^{-1} and the contour interval is $2x10^6$ m^2 s^{-1}. NCEP/NCAR reanalysis data 1979–99.

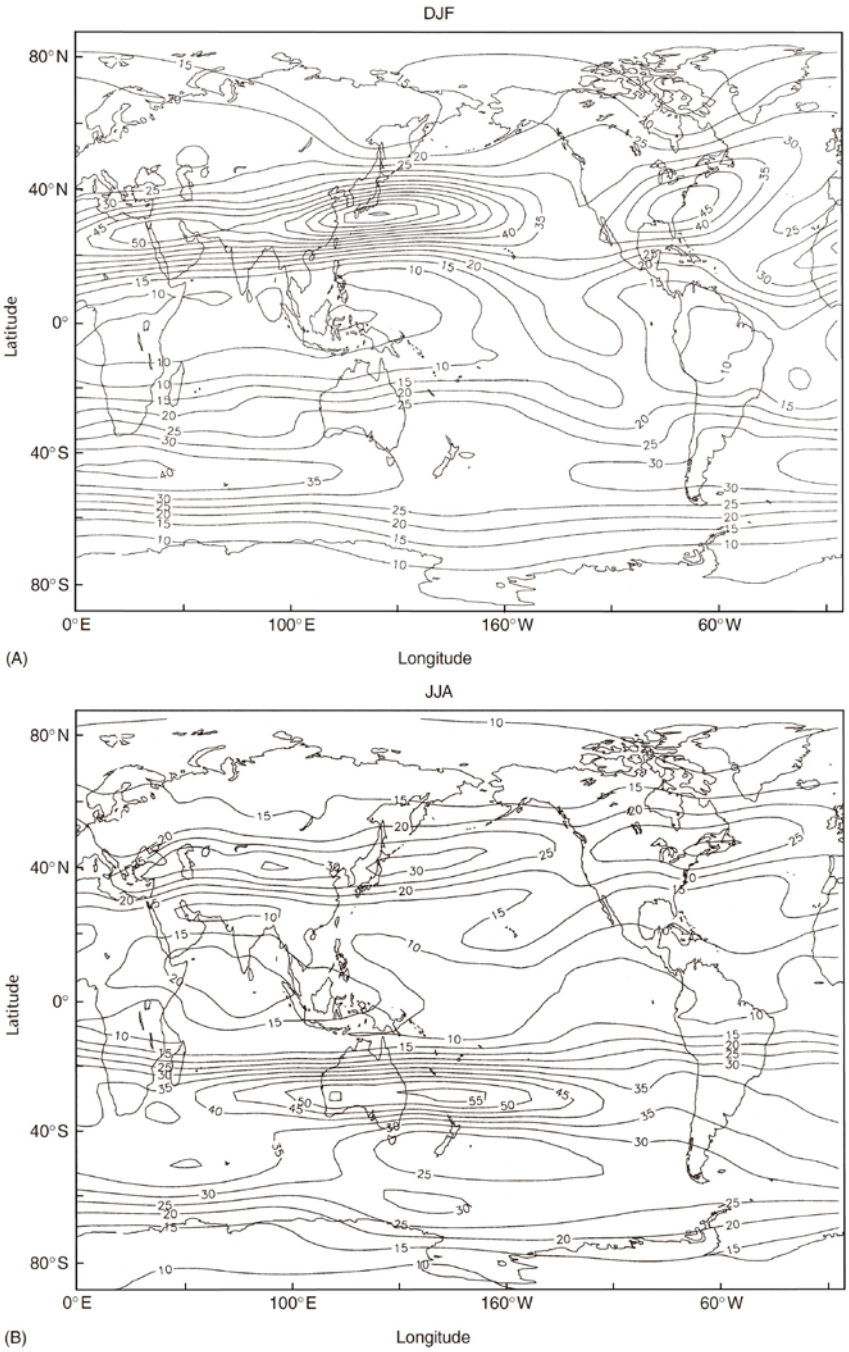

Figure 11 Time mean horizontal wind at 200 hPa for (A) December–February and (B) June–August. Contour interval is 5 m s^{-1}. NCEP/NCAR reanalysis data 1979–99.

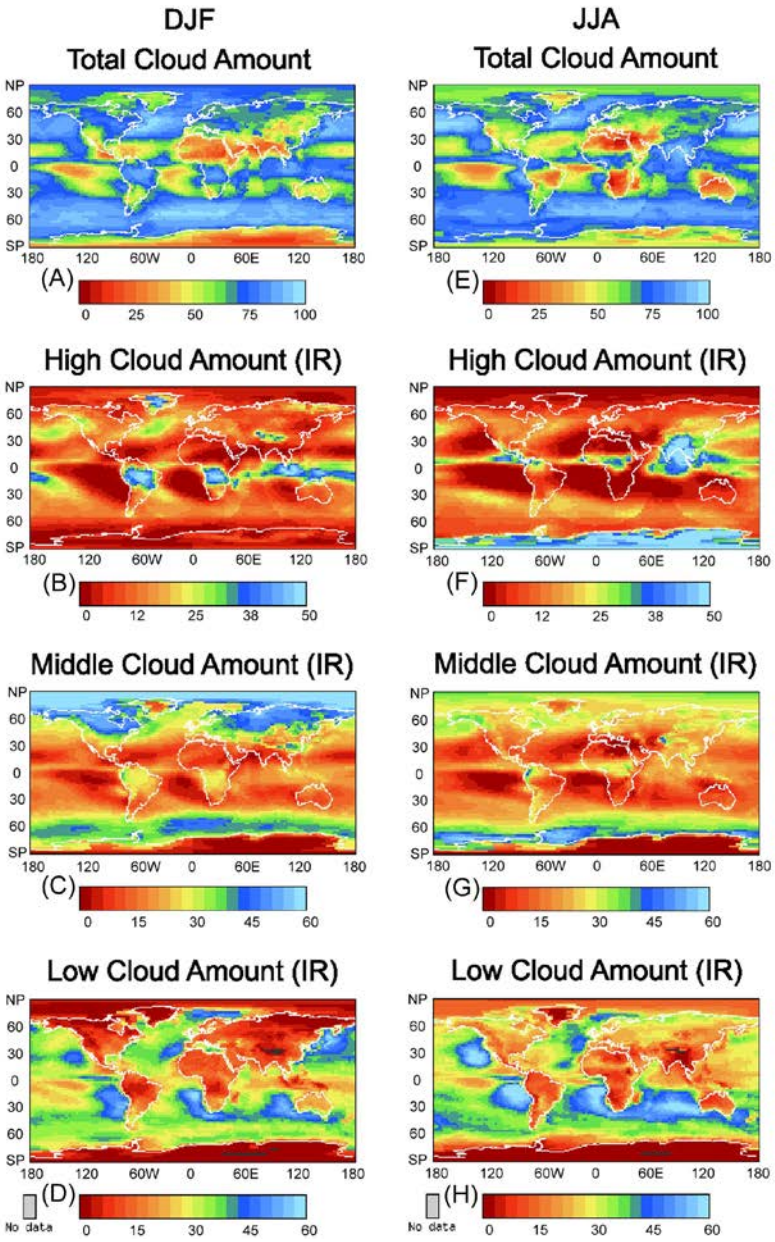

Figure 12 Cloud amount during December-February (left column) and June-August (right column). (A) and (E) Total amount at all levels. Estimates of average cloud amounts assigned to three general elevation ranges are also shown. (B) and (F) High clouds in the range 50-440 hPa. (C) and (G) Middle tropospheric clouds in the range of 440-680 hPa. (D) and (H) low level clouds below 680 hPa pressure surface elevation. Cloud amounts based on satellite estimates of the fraction of 5km wide pixels report cloud in each 280 km wide region. Geostationary and polar orbiting satellite data used, leading to some artificial boundary effects (e.g. Indian Ocean). Data are provided by the International Satellite Cloud Climatology Project (ISCCP) D2 monthly means combined from the July 1983 through June 2008 time period. If reproduced in grayscale, dark gray from few clouds, lightest gray for a middle amount of clouds for each indicated range, light inside darker gray for higher amounts in the range. Data maintained by the ISCCP research group at the NASA Goddard Institute for Space Studies, New York, NY. on January, 2005. Rossow, W.B., and Schiffer, R.A., 1999: Advances in Understanding Clouds from ISCCP. Bull. Amer. Meteor. Soc., 80, 2261-2288.

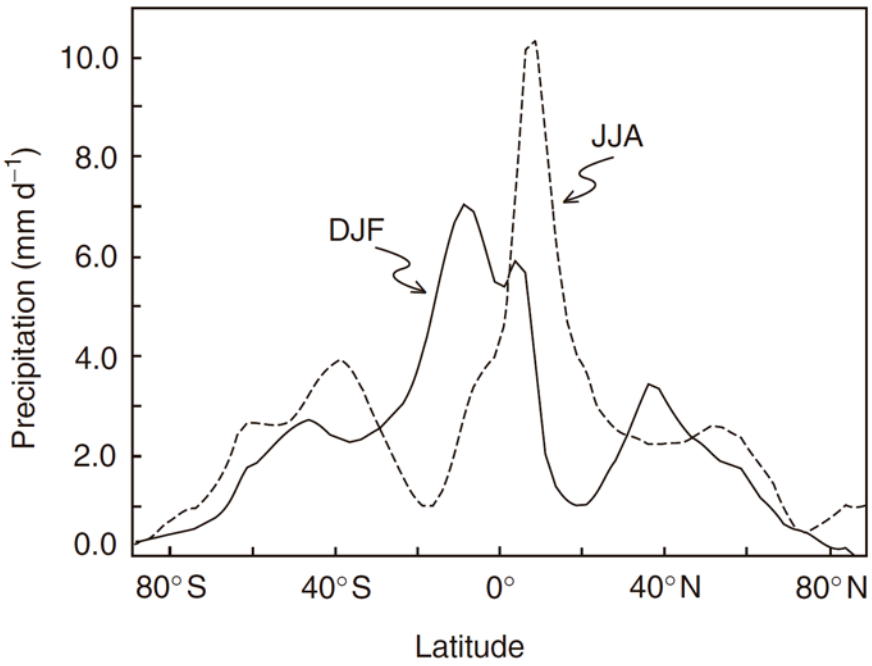

Figure 13 Zonal mean precipitation rate in mm/day for December – February (solid line) and June – August (dotted line). Climate Prediction Center Merged Analysis of Precipitation (CMAP) 1979–99 data used. Data provided by the NOAA/OAR/ESRL PSD, Boulder, Colorado, USA, from their Web site at http://www.esrl.noaa.gov/psd/.

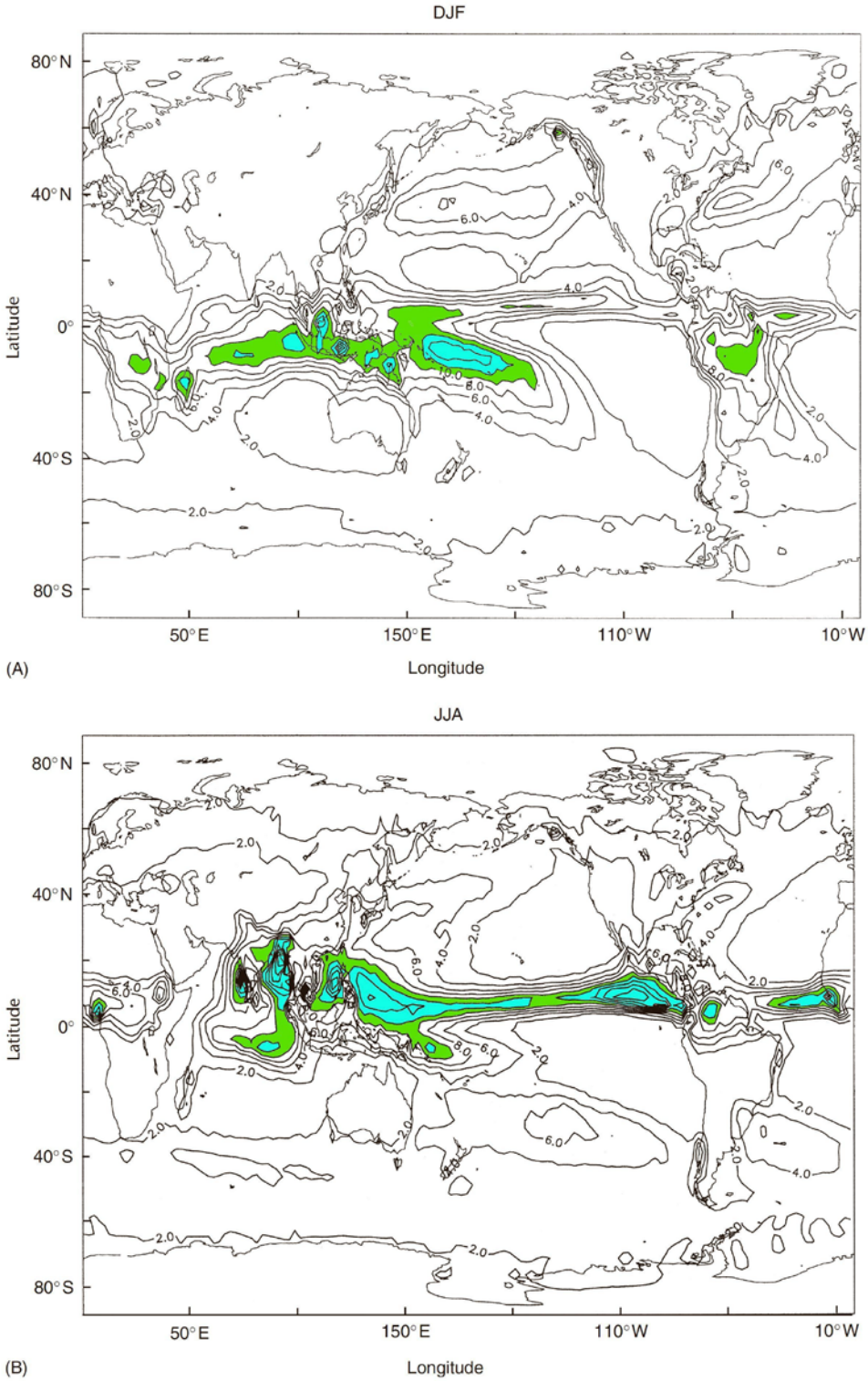

Figure 14 Time mean precipitation rate for (A) December–February and (B) June–August. Contour interval is 2mm day^{-1}. Values above 10 mm/day are shaded CMAP 1979–99 data used. Data provided by the NOAA/OAR/ESRL PSD, Boulder, Colorado, USA, from their Web site at http://www.esrl.noaa.gov/psd/.